Hemodynamic and Oxygen-metabolic Responses of the Awake Mouse Brain to Hypercapnia Revealed by Multi-parametric Photoacoustic Microscopy

Rui Cao[1], Angela Tran[2], Jun Li[3], Zhiqiang Xu[1], Naidi Sun[1,4], Zhiyi Zuo[3], and Song Hu[1,4]*

[1]Department of Biomedical Engineering, University of Virginia, Charlottesville, VA 22908

[2]Department of Biology, University of Virginia, Charlottesville, VA 22908

[3]Department of Anesthesiology, University of Virginia, Charlottesville, VA 22908

[4]Department of Biomedical Engineering, Washington University in St. Louis, St. Louis, MO 63130

*Correspondence:

Song Hu, Ph.D.

Washington University in St Louis

One Brookings Drive, Campus Box 1097

St. Louis, MO 63130

Tel: 314-935-3637

Email: songhu@wustl.edu

Running title: PAM of Cerebrovascular Responses to Hypercapnia

Abstract

A widely used cerebrovascular stimulus and common pathophysiologic condition, hypercapnia is of great interest in brain research. However, it remains controversial how hypercapnia affects brain hemodynamics and energy metabolism. By using multi-parametric photoacoustic microscopy, the multifaceted responses of the awake mouse brain to different levels of hypercapnia are investigated. Our results show significant and vessel type-dependent increases of the vessel diameter and blood flow in response to the hypercapnic challenges, along with a decrease in oxygen extraction fraction due to elevated venous blood oxygenation. Interestingly, the increased blood flow and decreased oxygen extraction are not commensurate with each other, which leads to reduced cerebral oxygen metabolism. Further, time-lapse imaging over 2-hour chronic hypercapnic challenges reveals that the structural, functional, and metabolic changes induced by severe hypercapnia (10% CO_2) are not only more pronounced but more enduring than those induced by mild hypercapnia (5% CO_2), indicating that the extent of brain's compensatory response to chronic hypercapnia is inversely related to the severity of the challenge. Offering quantitative, dynamic, and CO_2 level-dependent insights into the hemodynamic and metabolic responses of the brain to hypercapnia, these findings might provide useful guidance to the application of hypercapnia in brain research.

Keywords

Photoacoustic microscopy, hypercapnia, hemodynamics, oxygen metabolism, vascular response.

Introduction

Referring to the elevated carbon dioxide (CO_2) level in the blood, hypercapnia has long been used as a potent stimulus for the cerebral vasculature[1–3]. Even a small increase in the partial pressure of CO_2 (pCO_2) has noticeable impacts on the cerebral blood flow (CBF), due to its strong vasodilatory effect[4]. Because of its practicality, reliability, fast recovery, and low toxicity, hypercapnia has been widely used in cerebrovascular research[5–7]. Multiple approaches have been developed to induce hypercapnia, including holding breath[8,9], inspiring CO_2[10,11], and rebreathing exhaled gas[12].

Hypercapnia is the most commonly used stimulus for measuring cerebrovascular reactivity (CVR), which denotes the responsiveness of the cerebral vasculature to vasoactive challenges[13]. Readily measurable both experimentally and clinically, the CVR in response to hypercapnic challenges is an important indicator of cerebral perfusion reserve and vascular function and its alteration has been associated with multiple brain disorders, including ischemic stroke[14], brain tumor[15], traumatic brain injury[16,17], and Alzheimer's disease[18]. Understanding the response of the normal mouse brain to hypercapnia, as presented herein, will pave the way for follow-up studies in the diseased brain and will help the establishment and dissemination of CVR as a diagnostic marker.

Moreover, hypercapnia is widely used to calibrate functional magnetic resonance imaging (fMRI) for quantitative imaging of cerebral oxygen metabolism[19]. With the assumption that short-term hypercapnia alters CBF but not the cerebral metabolic rate of oxygen ($CMRO_2$), it has been used to calibrate the blood oxygen level-dependent (BOLD) signal against CBF[20]. Thus, quantitative assessments of the cerebral metabolic changes in response to hypercapnic challenges may facilitate the optimization of fMRI for $CMRO_2$ imaging with improved accuracy[21–23].

In recent years, photoacoustic microscopy (PAM) has drawn increasing attention and been widely applied in biomedical research[24,25]. Capable of imaging the optical absorption contrast acoustically, PAM combines the advantages of both optical imaging and ultrasound imaging[25,26]. Capitalizing on the strong optical absorption of hemoglobin in the visible range of the light spectrum, PAM is capable of imaging the vasculature *in vivo* at capillary-level resolution and in a label-free manner[27]. Through spectroscopic separation of oxy- and deoxy-hemoglobin (HbO_2 and HbR, respectively), the oxygen saturation of hemoglobin (sO_2) can be measured in individual microvessels[28]. Recent advances have enabled PAM to measure two other important hemodynamic parameters—the total

concentration of hemoglobin (C_{Hb}) and CBF[29]. By combining the simultaneously measured C_{Hb}, sO_2 and CBF, the multi-parametric PAM has demonstrated its ability to measure regional $CMRO_2$ in mice[30–32], making it an ideal tool to study the effects of hypercapnia on cerebral hemodynamics and oxygen metabolism.

In this work, we comprehensively characterized the multifaceted effects of hypercapnia on cerebral hemodynamics and oxygen metabolism in the mouse brain using the multi-parametric PAM. Given the fact that general anesthesia has strong influence on cerebral hemodynamics and activity, which is known to affect the metabolic response of the brain to hypercapnia[33], the head-restraint apparatus we previously developed for PAM of the awake brain was adopted. To avoid the out-of-focus issue when imaging across the uneven brain surface, the real-time contour-scanning strategy we recently developed was applied[34]. The structural (i.e., vessel diameter), functional (i.e., C_{Hb}, sO_2 and CBF), and oxygen-metabolic (i.e., oxygen extraction fraction (OEF) and $CMRO_2$) responses of the awake mouse brain to mild and severe hypercapnia (inhalation of 5% and 10% CO_2, respectively) were quantified and compared. The dependences of the responses on the vessel type (arteriole vs. venule) and diameter were studied.

Material and Methods

Animal preparation

Male CD-1 mice (9–12 weeks old, 35–45 grams, Charles River Laboratory) were used. All experimental procedures were carried out in conformity with the animal protocol approved by the Institutional Animal Care and Use Committee (IACUC) at the University of Virginia and were conducted in compliance with the Animal Welfare Act (AWA), National Institute of Health Guide for the Care and Use of Laboratory Animals, and ARRIVE (Animal Research: Reporting in Vivo Experiments) guideline 2.0[35]. One day prior to the experiment, a thinned-skull window was created under anesthesia with 1.5% isoflurane for optimal image quality. This one-hour anesthesia was not expected to have a strong residual effect on animal physiology, including cerebrovascular and metabolic responses, during the imaging studies that took place one day later. First, the scalp was shaved with an electric razor. Then, a 2.5-cm incision was made along the middle line. After the scalp was retracted to expose the region of interest (ROI), periosteum on the skull was remove

using a scalpel and a scissor. Following the established protocol[36], the skull was thinned down to ~100 μm using a surgical dental drill, during which saline flushing was performed periodically to prevent overheat and bleeding. After the window preparation, the mouse scalp was closed using surgical clips, and the incision was treated with povidone iodine to prevent infection. Before returning to its home cage, the animal was injected with 5mg/kg of ketoprofen subcutaneously for pain relief.

Photoacoustic microscopy of awake mouse brain

As shown in Supplementary Fig. S1, two ns-pulsed lasers (BX40-2-G, Edgewave) were used for photoacoustic excitation. To spectroscopically differentiate HbO_2 and HbR for sO_2 measurement, a polarization-maintaining single-mode fiber (F-SPA, Newport) was used to partially convert one laser output from 532 nm to 558 nm via the stimulated Raman scattering effect. The 558-nm Stokes light was isolated by a bandpass filter (FB560-10, Thorlabs) after the fiber output. Then, the two beams of different wavelengths were combined using a dichroic mirror (FF538-FDi01, Semrock) and coupled into the same single-mode fiber (P1-460B-FC-2, Thorlabs). A beam sampler (BSF10-A, Thorlabs) was placed before the fiber input to pick off ~5% of the light for real-time monitoring of the laser intensity fluctuation by a high-speed photodiode (FDS100, Thorlabs). The fiber output was mounted on the three-axis scanning head of the PAM system, where the dual-wavelength laser beam was collimated and then focused by a pair of achromatic doublets (AC127-025-A, Thorlabs). An iris (SM05D5, Thorlabs) was placed between the two doublets to control the beam width. The focused beam passed through the central opening of a ring-shaped ultrasonic transducer (inner and outer diameters: 2.2 and 4.0 mm, respectively; focal length: 6.0 mm; central frequency: 35 MHz; 6-dB intensity bandwidth: 70%) and was confocally aligned with the acoustic focus.

To avoid the out-of-focus problem caused by the uneven brain surface, our newly developed real-time contour-scanning strategy was used[34]. Briefly, the contour scan was implemented by moving the scanning head mounted on a vertical motorized stage along the curvature of the mouse brain. To achieve real-time contour scan without prior knowledge of the brain shape, the surface contour of the current B-scan was utilized to guide the contour scan of the next B-scan, which was adjacent

to the current B-scan with a small interval of 10 μm. More details can be found in our previous technical report[34].

To avoid the influence of general anesthesia on cerebral hemodynamics and oxygen metabolism, awake-brain imaging was carried out in this study. To secure the awake brain for high-resolution imaging, a nut was adhered to the skull contralateral to the ROI using dental cement about 6 hours before experiments. After cement solidification, the mouse head was fixed in a head-restraint apparatus using a screw and the mouse limbs were rested on an air-floated treadmill. The air pressure was adjusted to allow the mouse to move freely with a reduced reaction force for stress relief. To help the mouse acclimate to head restraint and relieve stress, each mouse was subjected to three training sessions before the imaging studies. Each session lasted for 45 minutes, during which the mouse was provided with drink as a positive reward. Animals with signs of pain or stress due to the restraint were excluded from the studies. Then, the mouse, along with the head-restraint apparatus, was placed under the scanning head of the PAM system. For acoustic coupling, a smear of ultrasound gel was applied between the thinned-skull window and a thin sheet of plastic wrap in the bottom of the water tank. The water was kept at 37 °C throughout the imaging period. The detailed procedure for PAM of the awake mouse brain has been previously reported by us[30].

Quantification of cerebral hemodynamics and oxygen metabolism

Capitalizing on the different optical absorption spectra of oxy- and deoxy-hemoglobin (HbO_2 and HbR, respectively), their relative concentrations ([HbR] and [HbO_2]) can be estimated based on a dual-wavelength PAM measurement. Using photoacoustic signals from two wavelengths (i.e., 532 nm and 558 nm), the sO_2 can be calculated as

$$sO_2 = \frac{[HbO_2]}{[HbR]+[HbO_2]}. \quad (1)$$

Consequently, the oxygen extraction fraction (OEF) in this region can be derived as

$$OEF = \frac{\overline{s_aO_2}-\overline{s_vO_2}}{\overline{s_aO_2}}, \quad (2)$$

where $\overline{s_aO_2}$ and $\overline{s_vO_2}$ are respectively the average sO_2 values of feeding arteries and draining veins.

Besides, the C_{Hb} can be quantified via statistical analysis of the amplitude fluctuation of the A-line signals acquired at 532 nm—a near-isosbestic point of hemoglobin. Briefly, the average count of RBCs within the detection volume of PAM can be estimated as

$$E(N_{RBC}) = \frac{E(Amp)}{Var(Amp) - Var(Noise)}, \tag{3}$$

where $E()$ and $Var()$ are the mean and variance operations, respectively, Amp is the amplitude of the PAM signal, and $Noise$ denotes the noise of the PAM system. Assuming each RBC contains ~15 pg of hemoglobin, the absolute C_{Hb} can be estimated as[29,37]

$$C_{Hb} = 15 \times \frac{E(N_{RBC})}{Vol}, \tag{4}$$

where Vol is the detection volume of the PAM system.

Furthermore, the blood flow speed can be quantified via correlation analysis of the PAM A-lines. As reported before[28], blood flow induces the decorrelation of sequentially acquired A-lines. Thus, the blood flow speed can be quantified by extracting the decay constant of the decorrelation curve. Then, the volumetric blood flow can be calculated by combining the flow speed revealed by the correlation analysis and the vessel diameter extracted from vessel segmentation[32]

$$Flow_v = \frac{\pi D^2 \bar{V}}{4}, \tag{5}$$

where D is the vessel diameter and $\bar{V}$ is the average flow speed within the vessel.

Based on all the hemodynamic parameters calculated above, the $CMRO_2$ can be derived by using Fick's law as

$$CMRO_2 = \xi \times C_{Hb} \times \overline{s_a O_2} \times OEF \times \frac{CBF_{total}}{W}, \tag{6}$$

where ξ is the oxygen binding capacity of hemoglobin (1.36 mL of oxygen per gram hemoglobin), CBF_{total} is the total volumetric blood flow through the ROI, and W is the tissue weight estimated by assuming an average cortical thickness of 1.2 mm[38] and a tissue density of 1.05 g/ml[39].

Hypercapnia model

To induce hypercapnia, the inhalation gas with preset CO_2 concentrations (5% and 10%) was used in this study. Different CO_2 concentrations were achieved by mixing pure CO_2 and medical air at

different flow rates regulated by separate flowmeters. The CO_2 concentration of the mixed gas was calibrated by using an anesthesia monitor (ULT KIT, Datex Engstrom).

Blood gas analysis

To confirm that the inhalation of 5% and 10% CO_2 induced different levels of hypercapnia, we collected arterial blood samples from the restrained awake mouse with a nosecone mask to prevent gas exchange with ambient air. The awake mouse was put into a tube-shaped animal holder with a small open window at the chest area, allowing convenient access to the heart of the restrained awake mouse. The tube-shaped animal holder has a nosecone mask at one end for CO_2 inhalation and a small hole at the other end for placement of the mouse tail to prevent the body movement. After 30-minute CO_2 inhalation, a cardiac puncture was performed using a 25-gauge syringe to draw blood from the left ventricle in the awake mouse. To alleviate potential pain, the mouse was subcutaneously injected with 0.25% bupivacaine in the chest area prior to the hypercapnic challenges. The collected blood (about 0.2 mL) was analyzed by a blood gas machine (IRMA, Diametrics Medical) to measure the arterial pCO_2 (i.e., $PaCO_2$) and pH. The animal was euthanized immediately after the blood collection.

Statistical analysis

One-way analysis of variance (ANOVA) and post hoc test was used in Figs. 3, 4, and 5 to show the structural, functional, and metabolic changes relative to their baseline values and also in Fig S4 to analyze the time dependence of the functional and metabolic changes. Also, two-way ANOVA with repeated measurement was used to compare the differential responses of the brain to mild vs. severe hypercapnia at each time point (Figs. 3 and 4) or within each vascular group (Fig. 5). Unpaired two-sample t-test was used in Fig. S2 and Fig. S3 to compare the measurements under different physiological conditions (i.e., normocapnia, mild hypercapnia, and severe hypercapnia). Note that a parametric or non-parametric test was selected based on a Kolmogorov–Smirnov test for normality to assess whether the data followed a normal distribution. All statistical data are presented in the format of mean ± standard deviation. P-values <0.05 were considered significant.

Results

Time-lapse imaging of dynamic cerebrovascular responses to hypercapnia

The cortical ROI of the awake mouse was repeatedly imaged by multi-parametric PAM to record the dynamic responses of cerebral hemodynamics and metabolism to hypercapnia. First, baseline images were taken under normocapnia. After the switch from medical air to the hypercapnic gas, time-lapse imaging was performed every 30 minutes for 2 hours.

To study the dose dependence of cerebrovascular responses to hypercapnia, two different levels of hypercapnia were induced in awake mice by inhalation of hypercapnic gas with 5% or 10% CO_2. As shown in Supplementary Fig. S2, after 30-minute inhalation of excessive CO_2, the blood pH dropped and the $PaCO_2$ elevated in both groups. Compared to the baseline (40.63±2.70 mmHg), the $PaCO_2$ increased to 58.53±3.89 mmHg (p<0.01) under mild hypercapnia and 83.10±7.88 mmHg (p<0.01) under severe hypercapnia (Supplementary Fig. S2a). Associated was decreases in the blood pH from 7.33±0.01 under normocapnia to 7.19±0.05 (p<0.01) under mild hypercapnia and to 7.09±0.02 (p<0.01) under severe hypercapnia (Supplementary Fig. S2b). Our results are in good agreement with recent studies in rats and piglets under similar hypercapnic challenges[40,41].

The arterial and venous sO_2 were readily distinguishable when the mouse was under normocapnia (Figs. 1 and 2). However, a noticeable elevation in the venous sO_2 was observed within 30-minute induction of mild hypercapnia (white arrows in Fig. 1), making it less distinguishable from the arterial sO_2. Accompanied were blood flow speed increase and arterial dilation (yellow arrows in Fig. 1), which together led to an increase in regional CBF. Continuous multi-parametric imaging over the 2-hour period of mild hypoxia shows a gradual renormalization of sO_2 and blood flow. Increases in the venous sO_2 and blood flow were also observed under severe hypercapnia (Fig. 2). However, in contrast to the hemodynamic renormalization after 120 minutes of mild hypercapnia, the venous sO_2 and blood flow remained noticeably higher than their baseline values throughout the 2-hour challenge with 10% CO_2 (white and yellow arrows in Fig. 2). Besides the hemodynamic changes, arterial dilation was also observed in response to severe hypercapnia.

Hypercapnia-induced changes in the cerebrovascular function

With the aid of vessel segmentation analysis, the average diameter, C_{Hb}, sO_2 and blood flow speed of individual microvessels in the ROI were quantified before and after the induction of hypercapnia, from which the percentage changes from their baseline values were calculated (Fig. 3). Note that there were no statistically significant differences between the baseline vascular parameters in the two groups of animals subject to mild or severe hypercapnia (Supplementary Fig. S3).

Significant and enduring arterial dilation was observed under both mild and severe hypercapnia (Fig. 3a), but the vasodilatory effect was more pronounced under severe hypercapnia [135.9±4.7% (p<0.01) of the baseline at 30 minutes and 131.8±5.9% (p<0.01) at 120 minutes] than mild hypercapnia [113.1±5.3% (p<0.01) at 30 minutes and 107.7±5.2% (p=0.026) at 120 minutes]. In contrast, enduring venous dilation was observed only under severe hypercapnia but not mild hypercapnia (Fig. 3b). The venous dilation maintained above 10% throughout the 2-hour period of severe hypercapnia [from 110.4±4.6% (p=0.011) of the baseline at 30 minutes to 113.5±6.9% (p=0.013) at 120 minutes], while the mild hypercapnia-induced venous dilation was rather transient and less pronounced—showing moderately enlarged diameter (104.6±3.5% of the baseline, p=0.04) at 30 minutes and returning to the baseline (100.9±2.0%, p=0.33) at 120 minutes. Inhalation of CO_2 also increased the blood flow speed (Fig. 3c). Similar to the venous dilation, the flow speed increase under severe hypercapnia [141.9±11.1% (p<0.01) of the baseline at 30 minutes and 129.3±10.4% (p<0.01) at 120 minutes] was more pronounced and enduring than that under mild hypercapnia [118.6±4.8% (p<0.01) at 30 minutes and 108.1±8.3% (p<0.01) at 120 minutes]. Also, the two-way ANOVA analysis showed that the CO_2 level was a major contributor to the differential responses in blood flow speed [$F(1, 8)=29.55$, p<0.01]. While the arterial sO_2 remained unchanged under both mild and severe hypercapnia (Fig. 3d), the venous sO_2 was significantly elevated under both conditions (126.1±14.6% (p<0.01) and 135.9±6.8% (p<0.01) of the baseline at 30 minutes under mild and severe hypercapnia, respectively). Similar to the blood flow speed, the venous sO_2 gradually returned to the baseline level (108.0±9.2% at 120 minutes, p=0.10) under mild hypercapnia (Fig. 3e). In contrast, the venous sO_2 remained significantly above the baseline throughout the 2-hour severe hypercapnia (131.9±7.9% at 120 minutes, p<0.01). It is worth noting that both time [$F(3, 24)=8.416$, p<0.01] and CO_2 levels [$F(1, 8)=12.98$, p<0.01] were significant factors underlying the changes in venous sO_2 and that there was a strong interaction between the two factors [$F(3, 24)=5.01$, p<0.01]. The C_{Hb} remained unchanged under mild hypercapnia, but slightly increased in the first 30 minutes of severe hypercapnia (113.9±5.6% of the baseline,

p<0.01) and then returned to the baseline level (Fig. 3f).

Hypercapnia-induced changes in the cerebral oxygen metabolism

Combining the structural and functional cerebrovascular parameters measured by multi-parametric PAM and quantified using the segmentation analysis, the regional CBF and OEF can be derived, from which the $CMRO_2$ can be estimated. The methodology for the quantification of CBF, OEF, and $CMRO_2$ is detailed in the section of Material and Methods.

As shown in Fig. 4a, a substantial and enduring increase in the regional CBF in response to severe hypercapnia was observed over the course of the 120-minute PAM monitoring [from 185.2±14.3% (p<0.01) of the baseline at 30 minutes to 174.7±13.4% (p<0.01) at 120 minutes]. In contrast, the CBF increase caused by mild hypercapnia was less pronounced and more transient [from 128.3±6.9% (p<0.01) at 30 minutes to 113.5±15.5% (p=0.19) at 120 minutes]. The two-way ANOVA analysis showed that both the CO_2 level [$F(1, 8)=65.84$, $p<0.01$] and time [$F(3, 24)=3.87$, $p=0.022$] have significant impacts on the changes in CBF. The increase in CBF was coupled with a drop in the regional OEF, which was mainly due to the increase of venous sO_2 since the arterial sO_2 remained unchanged. As shown in Fig. 4b, the OEF showed an abrupt decrease under both mild and severe hypercapnia [42.2±18.0% (p<0.01) and 10.5±6.3% (p<0.01) of the baseline at 30 minutes, respectively], followed by a gradual and hypercapnia level-dependent recovery [81.1±15.2% (p=0.047) and 24.4±20.9% (p<0.01) at 120 minutes for mild and severe hypercapnia]. Given the lack of changes in arterial sO_2 and C_{Hb}, $CMRO_2$ was proportional to the product of CBF and OEF, according to Eq. 6. Although the increased CBF and decreased OEF had opposite effects on $CMRO_2$, it resulted in a reduced $CMRO_2$ under hypercapnia, which indicates that OEF plays a dominant role. Interestingly, the amplitude and duration of the reduction are CO_2 level-dependent (Fig. 4c). Under mild hypercapnia, the $CMRO_2$ reduced to 56.9±23.1% (p=0.036) of the baseline in the first 30 minutes and then gradually returned to the baseline at 120 minutes (91.4±13.9%, p=0.18). In contrast, severe hypercapnia induced a more substantial initial decrease in the $CMRO_2$ (25.9±7.7%, p<0.01), which partially recovered over the 2-hour monitoring period but remained significantly lower than the baseline level (45.8±28.1% at 120 minutes, p=0.018). The two-way ANOVA analysis showed that the CO_2 level was a major contributor to the changes in both OEF [$F(1, 8)=21.12$, $p<0.01$] and $CMRO_2$ [$F(1, 8)=9.36$, $p=0.016$].

Vessel type-dependent responses to hypercapnia

According to Fig. 3, the difference in the acute cerebrovascular responses (i.e., 30 minutes) to mild and severe hypercapnia can be mainly attributed to that in the vessel diameter and blood flow. To investigate whether the differential responses are vessel type-dependent and, if so, which type(s) is most responsible, we classified the segmented vessels into four different categories based on the baseline diameter and sO_2 measured under normocapnia (large vessel vs. small vessel, and arteriole vs. venule). Vessels with a diameter less than 40 μm were considered small arterioles/venules[30,32].

As shown in Fig. 5a, within 30 minutes of CO_2 challenge, although all four types of cortical vessels underwent vasodilation in response to both levels of hypercapnia, the small arteriole was a major contributor to the differential responses [118.6±17.0% (p<0.01) under mild hypercapnia and 148.9±12.1% (p<0.01) under severe hypercapnia]. Similarly, small arterioles showed a more significant increase in flow speed in response to severe hypercapnia than mild hypercapnia (159.2±38.4% vs. 123.3±20.7%, p<0.01). In contrast, the flow speed increases in large arterioles under both levels of hypercapnia showed no difference (120.4±12.2% vs. 121.9±12.3%, p=0.77), as shown in Fig. 5b. Commensurate with the arteriolar flow increase were those in small and larger venues, both of which were significantly larger under severe hypercapnia. The increases in vessel diameter and flow speed together resulted in the elevation of volumetric blood flow (Fig. 5c), which again showed that the small arteriole is a major contributor to the hypercapnia level-dependent response [181.2±71.7% (p<0.01) and 355.3±93.7% (p<0.01)].

Discussion

Accounting for ~20% of the total oxygen consumption of the body at rest but lacking of ability to store oxygen, the brain relies on adequate blood supply to function properly[42]. The delicate balance between the energy demand imposed by neural activities and the oxygen supply provided by the blood circulation is maintained by ubiquitously presented microvessels in the brain. Subtle changes in the autoregulation of microvascular diameter, blood oxygenation, and/or blood flow can lead to severe problems in brain function and metabolism. Indeed, impairments of the CVR, particularly in the microvasculature, have been associated with a wide range of brain diseases, including stroke,

tumor, small vessel disease, traumatic brain injury, and Alzheimer's disease[13]. Thus, quantitative assessment of the CVR is crucial for understanding the vascular underpinning of brain physiology and pathology. Recent advances in fMRI have enabled single-vessel imaging at the mesoscopic level[43]; however, the CVR of small arterioles and venules remains inaccessible. More importantly, it remains a challenge to fully dissect and interpret the BOLD signal, which blends the multifaceted changes in sO_2, CBF, blood volume, and $CMRO_2$. Although allowing high-resolution imaging of the microvasculature[44,45], ultrasound localization microscopy and multi-photon microscopy (MPM) require angiographic agents and have limited accessibility to sO_2 (and thus OEF and $CMRO_2$). Uniquely capable of comprehensive imaging of microvascular blood perfusion, oxygenation, flow, and concomitant tissue oxygen extraction and metabolism[30,32], multi-parametric PAM is ideally suited for quantitative and comprehensive assessment of CVR.

Using multi-parametric PAM, we studied the effects of hypercapnia—a widely used physiological challenge for the CVR measurement[13]—on cerebral hemodynamics and oxygen metabolism in the awake mouse brain under the resting state. Our results provide microscopic insights into different aspects of CVR. Specifically, our data show multifaceted vascular reactivity of the awake mouse brain to hypercapnic challenges, including the increases in vessel diameter, flow speed, and venous sO_2. These vascular responses lead to increased regional CBF and decreased OEF, which, however, are not commensurate with each other and result in reduced $CMRO_2$.

Longitudinal monitoring of the cerebrovascular and metabolic responses to hypercapnia further reveal that they are dynamic and CO_2 level dependent. Specifically, the metabolic responses (*i.e.,* OEF and $CMRO_2$) of the awake mouse brain to 5% CO_2 were time-dependent and showed a gradual and significant recovery over the two-hour monitoring, in contrast to the moderate and statistically insignificant recovery under severe hypercapnia (Fig. S4). The multifaceted vascular and metabolic responses to mild hypercapnia (5% CO_2) are less pronounced and enduring than those to severe hypercapnia (10% CO_2). Also, the microscopic resolution of multi-parametric PAM and the segmentation-enabled single-vessel analysis together enable us to dissect the differential responses of arterioles and venules of different diameters to the different levels of hypercapnia, revealing that the small arteriole plays an essential role in the hypercapnia level-dependent CVR.

Our findings are in general agreement with earlier hypercapnia studies in both animals and humans. Specifically, the vasodilatory responses of the awake mouse brain to mild hypercapnia observed by multi-parametric PAM (13.1% in arterioles and 4.6% in venules) are in agreement with those observed by MPM (10.5% in arterioles and 4.1% in venules)[46]. Also, the mild hypercapnia-induced increase of blood flow speed in the awake mouse brain is observed by both PAM and laser speckle imaging (LSI)[46], although the increase observed in our study (18.6%) is larger than that in the LSI study (9.6%). Moreover, the mild hypercapnia-induced increase of venous sO_2 observed by PAM in the awake mouse brain (26.1%) is consistent with that observed by fMRI in the awake human brain (26.1% in Ref.[47] and 20.0% in Ref.[6]). Further, the predominant responses of small arterioles to hypercapnia observed by PAM echo previous observations by MPM in the awake mouse brain[46]. The gradual recovery of cerebral hemodynamics and metabolism during the 2-hour hypercapnia is in line with the previously reported compensatory response to chronic hypercapnia[48], and the more significant recovery under mild hypercapnia is in agreement with the previous observation that the extent of compensation is inversely related to the severity of hypercapnia[48]. Also, the hypercapnia level-dependent $CMRO_2$ suppression is consistent with the dose-dependent effect of hypercapnia on spontaneous neural activity observed in nonhuman primates by intracortical recording[49].

Although the mild hypercapnia-induced change in the venous sO_2 (also OEF, which can be directly derived from sO_2) measured by PAM agrees with that measured by fMRI, there is a considerable discrepancy in the observed CBF changes—28.3% increase in our PAM study vs. 54.5% or 63.3% in previous fMRI studies[6,47]. The discrepant findings might be partially attributed to the regional heterogeneity of brain's responses to hypercapnia[50]. Indeed, in our microscopic PAM study, CBF was measured over the motor cortex. While in the macroscopic fMRI studies, CBF was measured either in the superior sagittal sinus[47] or over the entire brain[6]. Thus, although with similar OEF measurements, the different readouts of the CBF response might lead to different findings of the effect of hypercapnia on $CMRO_2$.

Our findings of reduced $CMRO_2$ under hypercapnia is in general agreement with some previous findings in animals[51] and humans[47], despite other studies to the contrary[6,50]. However, the mild hypercapnia-induced $CMRO_2$ reduction observed by PAM (43.1%) in the awake mouse brain is higher than that observed by PET in the anesthetized nonhuman primate brain (29.4%)[51] and by fMRI in the awake human brain (13.4%)[47]. The discrepancy might be due to the differences in the

imaging methodology, the duration of the hypercapnic challenge, the use of anesthetic agents, the species studied, and the regional heterogeneity of brain's responses to hypercapnia.

The present study has limitations. The first lies in the imaging speed of the multi-parametric PAM. Due to the relatively low speed of the mechanical scan, the PAM system used in this study requires ~20 minutes to acquire a set of multi-parametric images. Thus, the duration of hypercapnia used in this study is much longer than that typically used in fMRI studies (3–5 minutes)[6,47], which may lead to different findings because acute increases in $PaCO_2$ have not shown significant reduction in $CMRO_2$ in normal humans[51]. Also, the long duration of hypercapnia with high $PaCO_2$ may lead to global cerebral edema and suppress the brain activity[13,52]. To improve the imaging speed of PAM, higher repetition-rate lasers and faster scanning mechanisms are needed. Our recent development has improved the imaging speed of multi-parametric PAM by 20-fold[55], enabling follow-up studies in the acute hypercapnia setting. It is worth noting that studies of cerebral blood flow dynamics in awake mice using optical coherence tomography and two-photon microscopy have been reported recently, providing alternative apporaches to study the brain responses to acute hypercapnia[53,54]. Second, the methods for the induction and maintenance of hypercapnia can be improved. Mixing CO_2 with air, which was previously used for fMRI studies[6], might lead to slightly reduced oxygen content in the gas mixture (20% and 19% O_2 in the mild and severe hypercapnia settings, respectively)[56]. Although there is no evidence that such mild hypoxia can influence the cerebral hemodynamics and metabolism, premixed hypercapnic gas with 21% O_2 should be used in future studies to avoid possible confounding effects[13]. Also, the hypercapnia level should be maintained by monitoring end-tidal pCO_2. Inspiration of CO_2 with a fixed concentration might induce variations in $PaCO_2$[7]. It is worth mentioning that the end-tidal pCO_2 measurement is more commonly used in hypercapnia studies because it is non-invasive and can be performed continuously. In this study, however, we measured the $PaCO_2$ instead due to the difficulty of measuring the end-tidal pCO_2 in awake mice. Thus, our reported $PaCO_2$ values under hypercapnia may be different from the end-tidal pCO_2 values reported in some previous studies[13]. Moreover, to ensure a consistent $PaCO_2$ level, dynamic end-tidal forcing and perspective end-tidal targeting techniques can be used[57–59], which, however, involves sophisticated airway control and gas delivery.

In summary, we have studied the cerebral hemodynamic and oxygen-metabolic responses to CO_2 inhalation-induced mild and severe hypercapnia in the awake mouse using multi-parametric PAM.

Our results show that both mild and severe hypercapnia (inducted by 5% and 10% CO_2 inhalation, respectively) can induce significant vasodilation, flow speed increase, and venous sO_2 elevation, which together result in increased CBF and decreased OEF. Instead of maintaining $CMRO_2$ at the level of normocapnia, the coupled changes in CBF and OEF are not commensurate with each other and lead to reduced regional $CMRO_2$, indicating that hypercapnia has a suppressive effect on brain activity and metabolism. Further, side-by-side comparison of the PAM readouts under mild and severe hypercapnia shows that cerebral hemodynamic and metabolic responses are hypercapnia level-dependent and that severe hypercapnia induces more pronounced and enduring responses. These findings may guide the application of CO_2 manipulation to assess cerebrovascular reactivity and the use of hypercapnia to calibrate fMRI signals. In addition, many patients with pulmonary diseases have CO_2 retention, our findings imply complex hemodynamic and metabolic changes in their brain.

Funding

The authors disclosed receipt of the following financial support for the research, authorship, and/or publication of this article: this study was supported by the National Institutes of Health (NS099261 and NS099118), the National Science Foundation (2023988), and the American Heart Association (15SDG25960005).

Declaration of conflicting interests

The author(s) declared no potential conflicts of interest with respect to the research, authorship, and/or publication of this article.

Authors' contributions

SH and RC conceived the study; RC and AT performed experiments and data analysis; RC and JL established the animal model and blood gas analysis; RC, ZX, and NS built the multi-parametric PAM system; RC, AT, ZZ, and SH wrote the manuscript.

Supplemental material

Supplementary material for this paper can be found at http://jcbfm.sagepub.com/content/by/supplemental-data

References

1. Ito H, Kanno I, Ibaraki M, et al. Changes in Human Cerebral Blood Flow and Cerebral Blood Volume during Hypercapnia and Hypocapnia Measured by Positron Emission Tomography. *J Cereb Blood Flow Metab* 2003; 23: 665–670.

2. Pollock JM, Deibler AR, Whitlow CT, et al. Hypercapnia-Induced Cerebral Hyperperfusion: An Underrecognized Clinical Entity. *AJNR Am J Neuroradiol* 2009; 30: 378–385.

3. Bishop C C, Powell S, Rutt D, et al. Transcranial Doppler measurement of middle cerebral artery blood flow velocity: a validation study. *Stroke* 1986; 17: 913–915.

4. Kety SS, Schmidt CF. The Effects of Altered Arterial Tensions of Carbon Dioxide and Oxygen on Cerebral Blood Flow and Cerebral Oxygen Consumption of Normal Young Men. *J Clin Invest* 1948; 27: 484–492.

5. Jones M, Berwick J, Hewson-Stoate N, et al. The effect of hypercapnia on the neural and hemodynamic responses to somatosensory stimulation. *NeuroImage* 2005; 27: 609–623.

6. Jain V, Langham MC, Floyd TF, et al. Rapid magnetic resonance measurement of global cerebral metabolic rate of oxygen consumption in humans during rest and hypercapnia. *J Cereb Blood Flow Metab* 2011; 31: 1504–1512.

7. Fierstra J, Sobczyk O, Battisti-Charbonney A, et al. Measuring cerebrovascular reactivity: what stimulus to use?: Measuring cerebrovascular reactivity. *The Journal of Physiology* 2013; 591: 5809–5821.

8. Hsu Y-Y, Chang C-N, Jung S-M, et al. Blood oxygenation level-dependent MRI of cerebral gliomas during breath holding. *Journal of Magnetic Resonance Imaging* 2004; 19: 160–167.

9. Li T-Q, Kastrup A, Takahashi AM, et al. Functional MRI of Human Brain during Breath Holding by BOLD and FAIR Techniques. *NeuroImage* 1999; 9: 243–249.

10. Dandona P, James IM, Newbury PA, et al. Cerebral blood flow in diabetes mellitus: evidence of abnormal cerebrovascular reactivity. *Br Med J* 1978; 2: 325–326.

11. Vernieri F, Tibuzzi F, Pasqualetti P, et al. Transcranial Doppler and near-infrared spectroscopy can evaluate the hemodynamic effect of carotid artery occlusion. *Stroke* 2004; 35: 64–70.

12. Read DC. A Clinical Method for Assessing the Ventilatory Response to Carbon Dioxide. *Australasian Annals of Medicine* 1967; 16: 20–32.

13. Liu P, De Vis JB, Lu H. Cerebrovascular reactivity (CVR) MRI with CO2 challenge: A technical review. *NeuroImage* 2019; 187: 104–115.

14. Geranmayeh F, Wise RJS, Leech R, et al. Measuring vascular reactivity with breath-holds after stroke: A method to aid interpretation of group-level BOLD signal changes in longitudinal fMRI studies. *Human Brain Mapping* 2015; 36: 1755–1771.

15. Fierstra J, van Niftrik B, Piccirelli M, et al. Altered intraoperative cerebrovascular reactivity in brain areas of high-grade glioma recurrence. *Magn Reson Imaging* 2016; 34: 803–808.

16. Kenney K, Amyot F, Haber M, et al. Cerebral Vascular Injury in Traumatic Brain Injury. *Experimental Neurology* 2016; 275: 353–366.

17. Cao R, Zhang C, Mitkin VV, et al. Comprehensive Characterization of Cerebrovascular Dysfunction in Blast Traumatic Brain Injury Using Photoacoustic Microscopy. *Journal of Neurotrauma* 2018; 36: 1526–1534.

18. Fleisher AS, Podraza KM, Bangen KJ, et al. Cerebral perfusion and oxygenation differences in Alzheimer's disease risk. *Neurobiology of Aging* 2009; 30: 1737–1748.

19. Gauthier CJ, Hoge RD. A generalized procedure for calibrated MRI incorporating hyperoxia and hypercapnia. *Hum Brain Mapp* 2013; 34: 1053–1069.

20. Davis TL, Kwong KK, Weisskoff RM, et al. Calibrated functional MRI: Mapping the dynamics of oxidative metabolism. *PNAS* 1998; 95: 1834–1839.

21. Hyder F, Kida I, Behar KL, et al. Quantitative functional imaging of the brain: towards mapping neuronal activity by BOLD fMRI. *NMR in Biomedicine* 2001; 14: 413–431.

22. Iannetti GD, Wise RG. BOLD functional MRI in disease and pharmacological studies: room for improvement? *Magnetic Resonance Imaging* 2007; 25: 978–988.

23. Strangman G, Culver JP, Thompson JH, et al. A Quantitative Comparison of Simultaneous BOLD fMRI and NIRS Recordings during Functional Brain Activation. *NeuroImage* 2002; 17: 719–731.

24. Xu M, Wang LV. Photoacoustic imaging in biomedicine. *Review of Scientific Instruments* 2006; 77: 041101.

25. Wang LV, Hu S. Photoacoustic Tomography: In Vivo Imaging from Organelles to Organs. *Science* 2012; 335: 1458–1462.

26. Wang LV, Yao J. A practical guide to photoacoustic tomography in the life sciences. *Nature Methods* 2016; 13: 627–638.

27. Maslov K, Zhang HF, Hu S, et al. Optical-resolution photoacoustic microscopy for *in vivo* imaging of single capillaries. *Opt Lett, OL* 2008; 33: 929–931.

28. Ning B, Kennedy MJ, Dixon AJ, et al. Simultaneous photoacoustic microscopy of microvascular anatomy, oxygen saturation, and blood flow. *Opt Lett, OL* 2015; 40: 910–913.

29. Ning B, Sun N, Cao R, et al. Ultrasound-aided Multi-parametric Photoacoustic Microscopy of the Mouse Brain. *Scientific Reports* 2015; 5: 18775.

30. Cao R, Li J, Ning B, et al. Functional and oxygen-metabolic photoacoustic microscopy of the awake mouse brain. *NeuroImage* 2017; 150: 77–87.

31. Cao R, Li J, Kharel Y, et al. Photoacoustic microscopy reveals the hemodynamic basis of sphingosine 1-phosphate-induced neuroprotection against ischemic stroke. *Theranostics* 2018; 8: 6111–6120.

32. Cao R, Li J, Zhang C, et al. Photoacoustic microscopy of obesity-induced cerebrovascular alterations. *NeuroImage* 2019; 188: 369–379.

33. Brevard ME, Duong TQ, King JA, et al. Changes in MRI signal intensity during hypercapnic challenge under conscious and anesthetized conditions. *Magnetic Resonance Imaging* 2003; 7.

34. Xu Z, Sun N, Cao R, et al. Cortex-wide multiparametric photoacoustic microscopy based on real-time contour scanning. *Neurophoton* 2019; 6: 1.

35. Percie du Sert N, Hurst V, Ahluwalia A, et al. The ARRIVE guidelines 2.0: Updated guidelines for reporting animal research. *J Cereb Blood Flow Metab* 2020; 40: 1769–1777.

36. Yang G, Pan F, Parkhurst CN, et al. Thinned-skull cranial window technique for long-term imaging of the cortex in live mice. *Nature Protocols* 2010; 5: 201–208.

37. Cao R, Li J, Zuo Z, et al. 10 - Photoacoustic Microscopy of Cerebral Hemodynamic and Metabolic Responses to General Anesthetics. In: Alfano RR, Shi L (eds) *Neurophotonics and Biomedical Spectroscopy*. Elsevier, pp. 215–227.

38. DeFelipe J. The Evolution of the Brain, the Human Nature of Cortical Circuits, and Intellectual Creativity. *Front Neuroanat*; 5. Epub ahead of print 16 May 2011. DOI: 10.3389/fnana.2011.00029.

39. Chong SP, Merkle CW, Leahy C, et al. Cerebral metabolic rate of oxygen (CMRO2) assessed by combined Doppler and spectroscopic OCT. *Biomed Opt Express* 2015; 6: 3941–3951.

40. Pourcyrous M, Chilakala S, Elabiad MT, et al. Does prolonged severe hypercapnia interfere with normal cerebrovascular function in piglets? *Pediatric Research* 2018; 84: 290–295.

41. Ding H, Liu X, Li X, et al. Hypercapnia exacerbates the disruption of the blood‐brain barrier by inducing interleukin‐1β overproduction in the blood of hypoxemic adult rats. *Int J Mol Med* 2020; 46: 762–772.

42. Jain V, Langham MC, Wehrli FW. MRI estimation of global brain oxygen consumption rate. *J Cereb Blood Flow Metab* 2010; 30: 1598–1607.

43. Yu X, He Y, Wang M, et al. Sensory and optogenetically driven single-vessel fMRI. *Nat Methods* 2016; 13: 337–340.

44. Errico C, Pierre J, Pezet S, et al. Ultrafast ultrasound localization microscopy for deep super-resolution vascular imaging. *Nature* 2015; 527: 499–502.

45. Wang T, Ouzounov DG, Wu C, et al. Three-photon imaging of mouse brain structure and function through the intact skull. *Nature Methods* 2018; 15: 789–792.

46. Nishino A, Takuwa H, Urushihata T, et al. Vasodilation Mechanism of Cerebral Microvessels Induced by Neural Activation under High Baseline Cerebral Blood Flow Level Results from Hypercapnia in Awake Mice. *Microcirculation* 2015; 22: 744–752.

47. Xu F, Uh J, Brier MR, et al. The Influence of Carbon Dioxide on Brain Activity and Metabolism in Conscious Humans: *Journal of Cerebral Blood Flow & Metabolism*. Epub ahead of print 15 September 2010. DOI: 10.1038/jcbfm.2010.153.

48. Eichenholz A, Blumentals AS, Walker FE. The pattern of compensatory response to chronic hypercapnia in patients with chronic obstructive pulmonary disease. *The Journal of Laboratory and Clinical Medicine* 1966; 68: 265–278.

49. Zappe AC, Uludağ K, Oeltermann A, et al. The Influence of Moderate Hypercapnia on Neural Activity in the Anesthetized Nonhuman Primate. *Cereb Cortex* 2008; 18: 2666–2673.

50. Chen JJ, Pike GB. Global Cerebral Oxidative Metabolism during Hypercapnia and Hypocapnia in Humans: Implications for BOLD fMRI. *J Cereb Blood Flow Metab* 2010; 30: 1094–1099.

51. Kliefoth AB, Grurb RL, Raichle ME. Depression of cerebral oxygen utilization by hypercapnia in the rhesus monkey. *Journal of Neurochemistry* 1979; 32: 661–663.

52. Zhou Q, Cao B, Niu L, et al. Effects of Permissive Hypercapnia on Transient Global Cerebral Ischemia–Reperfusion Injury in Rats. *Anesthesiology* 2010; 112: 288–297.

53. Erdener ŞE, Tang J, Sajjadi A, et al. Spatio-temporal dynamics of cerebral capillary segments with stalling red blood cells. *J Cereb Blood Flow Metab* 2019; 39: 886–900.

54. Şencan İ, Esipova T, Kılıç K, et al. Optical measurement of microvascular oxygenation and blood flow responses in awake mouse cortex during functional activation. *J Cereb Blood Flow Metab* 2020; 271678X20928011.

55. Wang T, Sun N, Cao R, et al. Multiparametric photoacoustic microscopy of the mouse brain with 300-kHz A-line rate. *NPh* 2016; 3: 045006.

56. Tancredi FB, Lajoie I, Hoge RD. A simple breathing circuit allowing precise control of inspiratory gases for experimental respiratory manipulations. *BMC Res Notes* 2014; 7: 235.

57. Wise RG, Pattinson KTS, Bulte DP, et al. Dynamic forcing of end-tidal carbon dioxide and oxygen applied to functional magnetic resonance imaging. *J Cereb Blood Flow Metab* 2007; 27: 1521–1532.

58. Alderliesten T, De Vis JB, Lemmers PMA, et al. Simultaneous quantitative assessment of cerebral physiology using respiratory-calibrated MRI and near-infrared spectroscopy in healthy adults. *NeuroImage* 2014; 85: 255–263.

59. Blockley NP, Driver ID, Francis ST, et al. An improved method for acquiring cerebrovascular reactivity maps. *Magn Reson Med* 2011; 65: 1278–1286.

Figure Captions

Fig. 1 Time-lapse PAM of sO_2 and blood flow speed during the 120-minute hypercapnic challenge induced by 5% CO_2 inspiration. The yellow and white arrows highlight changes in the arteriole and venule, respectively. Scale bar: 500 μm.

Fig. 2 Time-lapse PAM of sO_2 and blood flow speed during the 120-minute hypercapnic challenge induced by 10% CO_2 inspiration. The yellow and white arrows highlight changes in the arteriole and venule, respectively. Scale bar: 500 μm.

Fig. 3 Changes in the average (a) arteriole diameter, (b) venule diameter, (c) flow speed, (d) arterial sO_2, (e) venous sO_2, and (f) C_{Hb} over the 120-minute hypercapnic challenge induced by 5% or 10% CO_2 inhalation. Data are presented as mean ± SD (n=5). *, $p < 0.05$.

Fig. 4 Changes in (a) CBF, (b) OEF, and (c) $CMRO_2$ over the 120-minute hypercapnic challenge induced by 5% or 10% CO_2 inhalation. Data are presented as mean ± SD (n=5). *, $p < 0.05$.

Fig. 5 Vessel type-dependent responses of (a) vessel diameter, (b) flow speed, and (c) volumetric flow to hypercapnia within the first 30-minute inhalation of 5% or 10% CO_2. These vessels (20 small arterioles, 14 large arterioles, 15 small venules, and 19 large venules) were from five mice. Data are presented as mean ± SD. *, $p < 0.05$.

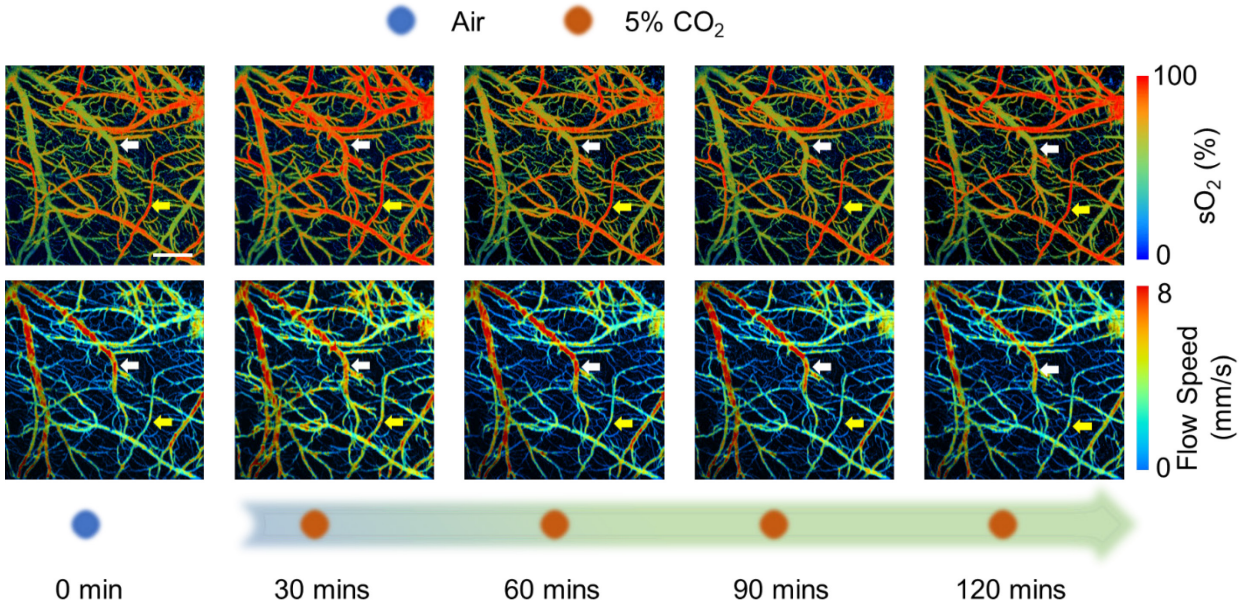
Air
5% CO_2
100
0
sO_2 (%)
8
0
Flow Speed (mm/s)
0 min
30 mins
60 mins
90 mins
120 mins

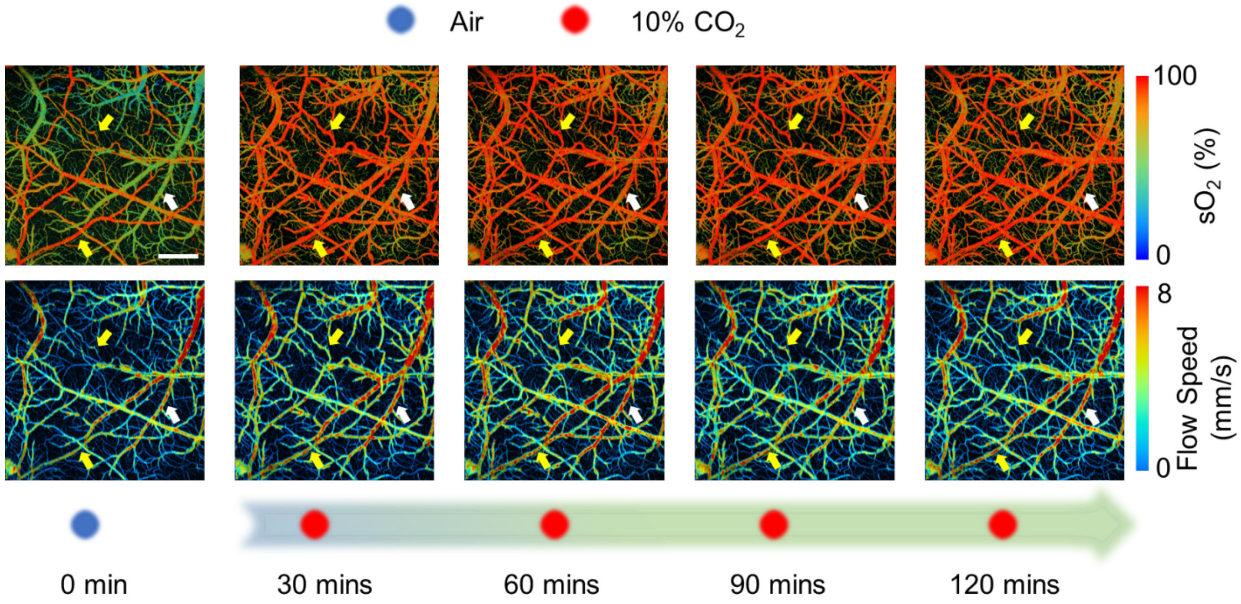
Air
10% CO_2
100
sO_2 (%)
0
8
Flow Speed (mm/s)
0
0 min
30 mins
60 mins
90 mins
120 mins

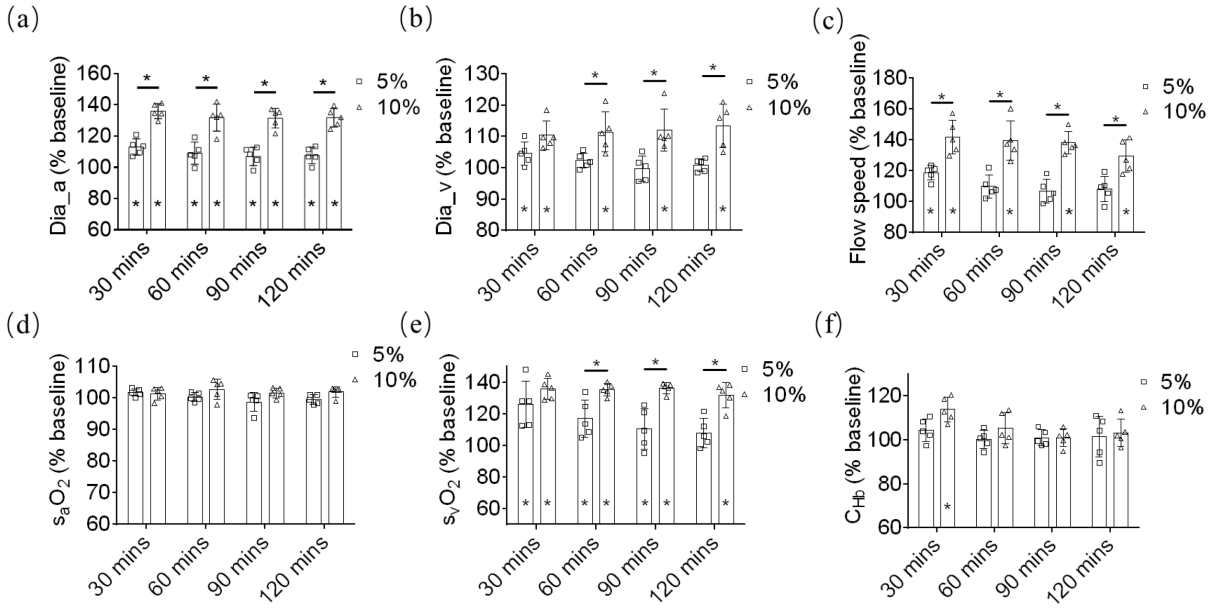
(a)
Dia_a (% baseline)
160
140
120
100
80
60
5%
10%
30 mins
60 mins
90 mins
120 mins
(b)
Dia_v (% baseline)
130
120
110
100
90
80
5%
10%
30 mins
60 mins
90 mins
120 mins
(c)
Flow speed (% baseline)
180
160
140
120
100
80
5%
10%
30 mins
60 mins
90 mins
120 mins
(d)
s_aO_2 (% baseline)
110
100
90
80
70
60
5%
10%
30 mins
60 mins
90 mins
120 mins
(e)
s_vO_2 (% baseline)
140
120
100
80
60
5%
10%
30 mins
60 mins
90 mins
120 mins
(f)
C_{Hb} (% baseline)
120
100
80
60
5%
10%
30 mins
60 mins
90 mins
120 mins

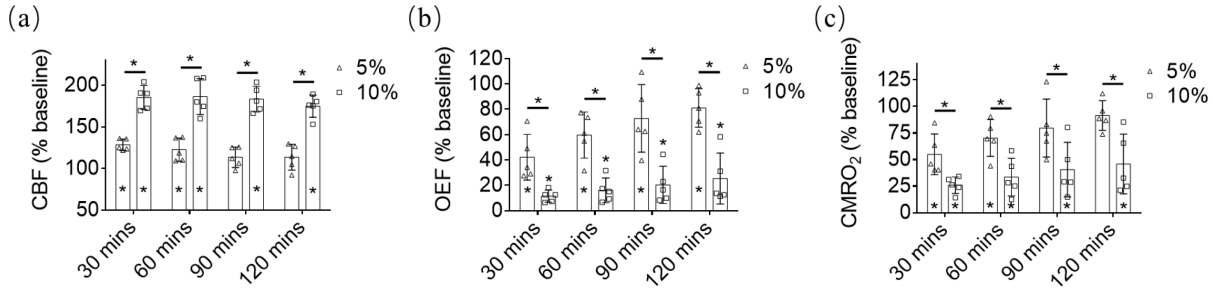
(a)
CBF (% baseline)
200
150
100
50
30 mins
60 mins
90 mins
120 mins
5%
10%
(b)
OEF (% baseline)
120
100
80
60
40
20
0
30 mins
60 mins
90 mins
120 mins
5%
10%
(c)
CMRO2 (% baseline)
125
100
75
50
25
0
30 mins
60 mins
90 mins
120 mins
5%
10%

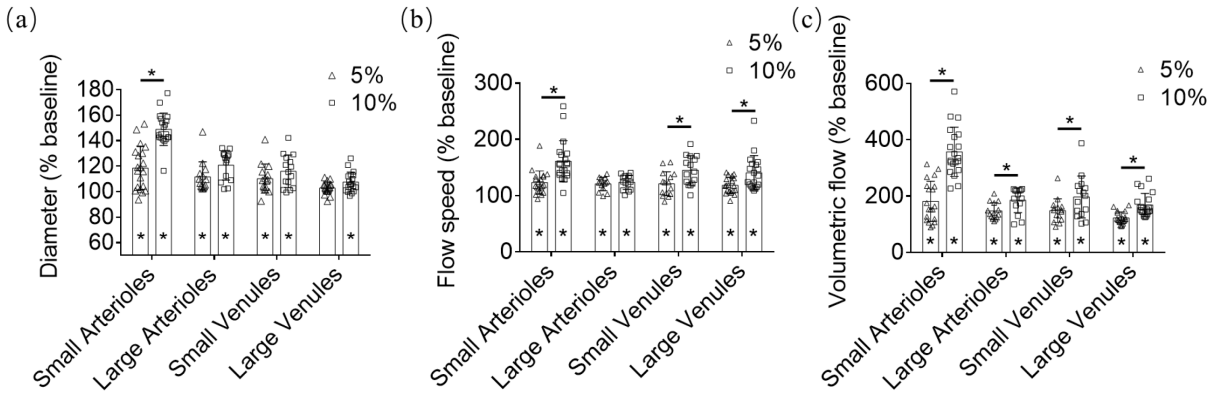
(a)
Diameter (% baseline)
180
160
140
120
100
80
60
5%
10%
Small Arterioles
Large Arterioles
Small Venules
Large Venules
(b)
Flow speed (% baseline)
300
200
100
0
5%
10%
Small Arterioles
Large Arterioles
Small Venules
Large Venules
(c)
Volumetric flow (% baseline)
600
400
200
0
5%
10%
Small Arterioles
Large Arterioles
Small Venules
Large Venules